DALTON

Syntheses, crystal structures, and electrochemical and spectroscopic properties of ruthenium complexes of the N,S-bidentate ligand 2-(2-pyridyl)benzenethiol

Alexander M. W. Cargill Thompson, David A. Bardwell, John C. Jeffery, Leigh H. Rees and Michael D. Ward*

School of Chemistry, University of Bristol, Cantock's Close, Bristol BS8 1TS, UK

Conversion of the amino group of 2-(2-aminophenyl)pyridine into a thiol to give the N,S-donor chelating ligand 2-(2-pyridyl)benzenethiol (HL) afforded the oxidised disulfide L–L which was crystallographically characterised. It shows an interesting example of an intermolecular N · · · S–S interaction (N · · · S distances are 2.778 and 2.724 Å; N · · · S–S angles are both *ca.* 11°) in which the pyridyl lone pair interacts weakly with the σ* orbital of the S–S bond. Reaction of L–L with $[Ru(bipy)_2Cl_2]\cdot 2H_2O$ (bipy = 2,2′-bipyridine) and $RuCl_3\cdot xH_2O$ afforded $[Ru^{II}(bipy)_2L][PF_6]$ **1** and $[Ru^{III}L_3]$ **2** respectively (following *in situ* reduction of the disulfide) which have N_5S and *mer*-N_3S_3 donor sets respectively (N of pyridyl, S of benzenethiolate). Both were crystallographically characterised and have the expected pseudo-octahedral geometries. An interesting feature of both structures is that the relatively large Ru–S distances (compared to the Ru–N) prevent the pyridyl rings from approaching the metal centre as closely as they would if they were not constrained, so the Ru–N distances are longer than usual. Electrochemical studies show that the benzenethiolate ligands are more effective electron donors to ruthenium (both +2 and +3) than are phenolates: for example, the Ru^{II}–Ru^{III} couple of **1** is at −0.07 V *vs.* ferrocene–ferrocenium, whereas the same couple of the related N_5O-co-ordinated complex (O from phenolate) was at +0.03 V. Similarly the Ru^{III}–Ru^{IV} couple of **2** was at −0.21 V, compared to +0.14 V for the N_3O_3-co-ordinated analogue. Complex **2** also shows a reversible ligand-based oxidation which is absent for **1**, arising from stabilisation of the sulfur-based radical cation by interaction with the lone pair on an adjacent sulfur atom in the co-ordination sphere of the complex, which cannot happen for **1**. Electronic spectral properties show that the sulfur donor of **1** weakens the ligand field with respect to $[Ru(bipy)_3]^{2+}$, and that **2** has an intense sulfur-to-Ru^{III} ligand-to-metal charge-transfer band.

As part of our continuing study on new mixed-donor polydentate ligands,[1] we describe in this paper the synthesis and some co-ordination chemistry of the simple N,S-bidentate chelating ligand 2-(2-pyridyl)benzenethiol (HL). Complexes containing sulfur donors are of biological relevance since they can model the co-ordination of cysteine and/or methionine residues which occurs in a wide variety of metalloproteins such as rubredoxins and ferredoxins, nickel hydrogenases, type I copper proteins, various molybdenum oxidases, the iron/molybdenum nitrogenases and the zinc 'finger' proteins.[2] Amongst these, examples of complexes containing benzenethiolate donors[3] are somewhat rarer than those based on aliphatic thiolates or thioethers.

We focus in this paper on the mononuclear ruthenium complexes $[Ru^{II}(bipy)_2L][PF_6]$ **1** (bipy = 2,2′-bipyridine) and $[Ru^{III}L_3]$ **2**, both of which have mixed pyridine–benzenethiolate donor sets. The chemistry of ruthenium benzenethiolates in oxidation states +2 to +4 is well-established.[4] However systematic studies of their electrochemical and spectroscopic properties as a function of ligand donor set[5] are not as well established as they are for ruthenium complexes with other ligands, for which it is well known that strong correlations between the donor set and the electrochemical and spectroscopic properties of the metal centre exist.[6–9] We have previously studied ruthenium complexes of the analogous pyridine–phenol ligand 2-(2-hydroxyphenyl)pyridine (Hhpp),[6,7] and the comparison between the electronic properties of phenolate and benzenethiolate ligands will also be of interest.

Experimental

General details

The following instruments were used for routine spectroscopic studies: ^{1}H NMR spectroscopy, a JEOL λ-300 spectrometer; electron impact (EI), chemical ionisation (CI) and positive-ion fast-atom bombardment (FAB) mass spectra, a VG-Autospec; UV/VIS spectra, Perkin-Elmer Lambda-2 or -19 instruments. Electrochemical measurements were made with an EG&G PAR 273A potentiostat, using platinum-bead working and auxiliary electrodes, and a saturated calomel reference electrode (SCE). The measurements were performed using acetonitrile distilled over calcium hydride, with 0.1 mol dm^{-3} $[NBu^n_4][PF_6]$ as supporting electrolyte. Ferrocene was added at the end of each experiment as an internal reference, and all redox potentials are quoted *vs.* the ferrocene–ferrocenium couple.

2-(2-Aminophenyl)pyridine[10] and $[Ru(bipy)_2Cl_2]\cdot 2H_2O$ (bipy = 2,2′-bipyridine)[11] were prepared according to published methods.

Syntheses

Bis[2-(2-pyridyl)phenyl] disulfide (L–L). This preparation is based on a published procedure.[12] 2-(2-Aminophenyl)pyridine (1.65 g, 9.71 mmol) in water (10 cm^3) and concentrated hydrochloric acid (2 cm^3) was cooled to 0 °C and diazotised by adding $NaNO_2$ (0.86 g, 12.5 mmol) in small portions over 20 min. This diazonium salt solution was added over 30 min to a solution of potassium *O*-ethyl dithiocarbonate (3.8 g, 29.5 mmol, excess) in water (15 cm^3) at 60 °C, and stirring was then continued at this temperature for 30 min. On cooling, the resulting oil was extracted with CH_2Cl_2, the organic extracts were dried over $MgSO_4$ and the solvent was removed *in vacuo*. The oil was added to ethane-1,2-diamine (15 cm^3) and stirred under nitrogen at room temperature for 16 h. The reaction mixture was then quenched with water (50 cm^3) and neutralised by careful addition of concentrated hydrochloric acid. The crude product was extracted with CH_2Cl_2, and the organic extracts were dried

($MgSO_4$) and reduced to an oil. Column chromatography on alumina (Brockmann grade approximately 3) eluting with CH_2Cl_2 afforded bis[2-(2-pyridyl)phenyl] disulfide (L–L), which followed an initial, fast-moving, yellow impurity. Removal of the solvent *in vacuo*, followed by recrystallisation from hot toluene, afforded the disulfide as pale yellow crystals (0.71 g, 39%) suitable for an X-ray diffraction study. EI and CI mass spectra: *m/z* 186, $[L]^+$ (Found: C, 71.0; H, 4.5; N, 7.5. Calc. for $C_{22}H_{16}N_2S_2$: C, 70.9; H, 4.3; N, 7.5%). ^{1}H NMR ($CDCl_3$, 300 MHz): δ 8.73 (ddd, 1 H, pyridyl H^6), 7.79 (m, 2 H, pyridyl H^4 and phenyl H^3 or H^6), 7.61 (ddd, 1 H, pyridyl H^3), 7.50 (m, 1 H, phenyl H^6 or H^3) and 7.29 (m, 3 H, pyridyl H^5 and phenyl H^4 and H^5).

$[Ru^{II}(bipy)_2L][PF_6]$ 1. The compound L–L (0.060 g, 0.16 mmol) and $[Ru(bipy)_2Cl_2]\cdot 2H_2O$ (0.167 g, 0.32 mmol) were heated at reflux in 1:1 aqueous methanol (20 cm^3) for 1 h. The solution changed from deep purple to black. The reaction mixture was cooled and the crude $[Ru^{II}(bipy)_2L]^+$ was precipitated as the hexafluorophosphate salt by addition of an excess of aqueous KPF_6. The brown-black precipitate was collected on Celite, washed with a little water, and redissolved in the minimum volume of MeCN. Column chromatography on flash-grade silica, eluting with acetonitrile–saturated aqueous KNO_3–water (28:2:1 v/v) afforded **1** as a fast-moving dark band which was followed by slower-moving orange impurities. Addition of an excess of aqueous KPF_6 to the product fraction and reduction in volume afforded a green-black precipitate which was recrystallised from aqueous acetonitrile, washed with water and diethyl ether, and dried (0.160 g, 67%). Anion metathesis of $[Ru(bipy)_2L][PF_6]$ with an excess of $NaBF_4$ in aqueous MeCN afforded $[Ru(bipy)_2L][BF_4]$ **1a** which gave X-ray-quality crystals on diffusion of diethyl ether vapour into a concentrated acetonitrile solution. FAB mass spectra: *m/z* 600, $[M - PF_6]^+$ (Found for **1**: C, 50.3; H, 3.2; N, 9.5. Calc. for $C_{31}H_{24}F_6N_5PRuS$: C, 50.0; H, 3.2; N, 9.4%). ^{1}H NMR (CD_3CN, 400 MHz): δ 9.60 (ddd, 1 H, H^{6a}), 8.62 (d, 1 H, H^{3a}), 8.53 (d, 1 H, H^{3b}), 8.29 (ddd, 1 H, H^{6e}), 8.22 (d, 1 H, H^{3d}), 8.15 (d, 1 H, H^{3e}), 8.10 (ddd, 1 H, H^{4a}), 7.93 (ddd, 1 H, H^{6b}), 7.87 (ddd, 1 H, H^{4b}), 7.72 (m, 3 H, H^{4c}, H^{4d}, H^{4e}), 7.62 (dd, 1 H, H^{3c}), 7.52 (ddd, 1 H, H^{5a}), 7.30 (dd, 1 H, H^{3f}), 7.20 (m, 2 H, H^{5b}, H^{6d}), 7.14 (ddd, 1 H, H^{6c}), 7.22 (m, 3 H, H^{5d}, H^{5e}, H^{4f}), 6.96 (d, 1 H, H^{6f}) and 6.78 (m, 2 H, H^{5c}, H^{5f}) (where a–f denote the six aromatic rings).

$[Ru^{III}L_3]$ 2. The compound L–L (0.106 g, 0.285 mmol) and $[Ru(acac)_3]$ (acac = acetylacetonate) (0.057 g, 0.142 mmol) were heated at reflux in ethane-1,2-diol (10 cm^3) for 3 h with nitrogen being bubbled slowly through the reaction mixture throughout. The original pink colour changed to green when the mixture reached reflux. After cooling, water (60 cm^3) was added and the mixture was extracted with CH_2Cl_2 (4 × 30 cm^3). The green-brown extracts were dried ($MgSO_4$), the solvent was evaporated, and the residue chromatographed on alumina (Brockmann grade 3), eluting with CH_2Cl_2. A minor pale yellow impurity was eluted first, followed by the main green product band. The clean product fractions were combined, reduced to dryness and reprecipitated from CH_2Cl_2–hexane, affording $[RuL_3]$ as a brown-green powder (0.051 g, 54%). Crystals suitable for X-ray crystallographic structure determination were grown by diffusion of ether into a CH_2Cl_2 solution of $[RuL_3]$. FAB mass spectrum: *m/z* 660, $[M]^+$; 474 $[M - L]^+$ (Found: C, 59.9; H, 3.6; N, 6.1. Calc. for $C_{33}H_{24}N_3RuS_3$: C, 60.1; H, 3.7; N, 6.4%).

Crystallography

Suitable crystals were mounted on a brass pin in a stream of N_2 at −100 °C on the diffractometer as quickly as possible to prevent possible decomposition due to loss of lattice solvent. Data were collected at −100 °C using a Siemens SMART three-circle diffractometer with a CCD area detector (graphite-monochromatised Mo-Kα X-radiation, $\bar{\lambda} = 0.710\,73$ Å). Data were corrected for Lorentz-polarisation effects, and for absorption effects by an empirical method based on multiple measurements of equivalent data. Details of the crystal parameters, data collection and refinement are in Table 1. The structures were solved by conventional heavy-atom or direct methods (SHELXTL)[13] and were refined by the full-matrix least-squares method on all F^2 data (SHELXTL)[13] using a Silicon Graphics Indigo R4000 computer. All non-hydrogen atoms were refined anisotropically; hydrogen atoms were included in calculated positions and refined with isotropic thermal parameters.

Crystals of compound **1a** had the chiral space group $P2_12_12_1$. However they formed 1:1 racemic twins, so although the structure could be solved and refined adequately the absolute configuration of the complex cation was indeterminable. The rather high residual peaks in the final electron-density map were close to the ruthenium atom, and arise from the difficulties associated with applying an accurate absorption correction to a needle-like crystal. Crystals of L–L and **2**·$0.5CH_2Cl_2$ presented no problems.

Table 1 Crystallographic data for L–L, **1a** and **2**·$0.5CH_2Cl_2$

	L–L	**1a**	**2**·$0.5CH_2Cl_2$
Formula	$C_{22}H_{16}N_2S_2$	$C_{31}H_{24}BF_4N_5RuS$	$C_{33.5}H_{25}ClN_3RuS_3$
M	372.49	686.49	702.27
System, space group	Monoclinic, $P2_1/n$	Orthorhombic, $P2_12_12_1$	Monoclinic, $C2/c$
a/Å	10.648(1)	12.182(4)	34.800(10)
b/Å	11.184(2)	13.545(6)	10.855(2)
c/Å	15.463(3)	17.223(5)	16.137(2)
β/°	90.026(10)	—	99.44(3)
U/Å^3	1841.4(5)	2842(2)	6013(2)
Z	4	4	8
D_c/g cm^{-3}	1.344	1.605	1.552
μ/mm^{-1}	0.297	0.683	0.848
F(000)	776	1384	2848
Crystal size/mm	0.6 × 0.5 × 0.3	0.4 × 0.1 × 0.1	0.5 × 0.2 × 0.1
2θ range for data collection/°	4–50	4–50	4–50
Reflection collected (total, independent, R_{int})	8360, 3211, 0.020	13566, 4991, 0.076	13981, 5224, 0.049
Data, restraints, parameters	3211, 0, 251	4991, 0, 389	5215, 2, 378
Final: *R*1, *wR2*[a,b]	0.0288, 0.0825	0.0643, 0.1619	0.0474, 0.1180
Weighting factors (*a*, *b*)[b]	0.0455, 0.6755	0.1006, 0	0.0355, 43.7098
Largest peak, hole/e Å^{-3}	+0.198, −0.252	+1.909, −2.576	+1.069, −0.969

[a] Structure was refined on F_o^2 using all data; the value of *R*1 is given for comparison with older refinements based on F_o with a typical threshold of $F \geqslant 4\sigma(F)$. [b] $wR2 = [\Sigma w(F_o^2 - F_c^2)^2/\Sigma w(F_o^2)^2]^{\frac{1}{2}}$ where $w^{-1} = \sigma^2(F_o^2) + (aP)^2 + bP$ and $p = [\max(F_o^2,0) + 2F_c^2]/3$.

Atomic coordinates, thermal parameters, and bond lengths and angles have been deposited at the Cambridge Crystallographic Data Centre (CCDC). See Instructions for Authors, *J. Chem. Soc., Dalton Trans*, 1997, Issue 1. Any request to the CCDC for this material should quote the full literature citation and the reference number 186/349.

Results and Discussion

Syntheses

The compound HL was mentioned a few years ago as an intermediate in the synthesis of a fused isothiazoles,[12] and is prepared by conversion of the amino group of the known compound 2-(2-aminophenyl)pyridine (an interesting bidentate ligand in its own right)[14] into a thiol by reaction with potassium *O*-ethyl dithiocarbonate. However in the original report the compound was obtained crude and not purified or characterised. We found that following chromatographic purification it was isolated as the crystalline disulfide L–L, which is a convenient (and relatively odourless!) way of storing it, especially as it can be used directly to prepare the ruthenium complexes **1** and **2** without the need for initial regeneration of the thiol HL in a separate step.

Reaction of L–L with $[Ru(bipy)_2Cl_2]\cdot 2H_2O$ in aqueous methanol at reflux resulted in reduction of the disulfide and co-ordination of anionic, bidentate L^- to the metal centre to give the complex $[Ru^{II}(bipy)_2L][PF_6]$ **1**, with an N_5S donor set. Following chromatographic purification, **1** was characterised on the basis of its FAB mass spectrum, which gave a strong peak for the complex monocation, and elemental analysis. In addition the ^{1}H NMR spectrum showed the presence of 24 inequivalent proton environments in the aromatic region. The spectrum has not been fully assigned, but with the aid of two-dimensional ^{1}H–^{1}H correlation spectroscopy (COSY) the signals could be separated into six sets of four, corresponding to the six aromatic rings (see Experimental section). We could not grow X-ray-quality crystals of **1**, so a small portion was converted into the $[BF_4]^-$ salt **1a**, which did give such crystals from $MeCN–OEt_2$.

The homoleptic complex $[Ru^{III}L_3]$ **2**, with an N_3S_3 donor set, was prepared by reaction of L–L with $[Ru(acac)_3]$ in ethylene glycol at high temperatures. Under these conditions the anionic acac ligands protonate and are lost from the reaction mixture by evaporation of neutral Hacac, and this strategy has been successful for preparing a variety of homoleptic ruthenium(III) complexes with bidentate chelating ligands.[15] Again the disulfide L–L reduces *in situ* to produce $[L]^-$, which co-ordinates. In contrast, reaction of an excess of ligand with a starting material such as ruthenium trichloride tends to yield mixtures of partially reacted materials in which chloride ions are still co-ordinated to the metal. Again initial characterisation was on the basis of FAB mass spectrometry and elemental analysis.

Crystal structures

The structure of the disulfide dimer L–L is shown in Fig. 1; selected bond lengths and angles are in Table 2. Apart from confirming that oxidation to the disulfide had indeed occurred (which could not be proved conclusively from the spectroscopic or analytical data), two features of the structure are worth commenting on. First, the torsion angles between the pyridyl and phenyl rings are rather smaller than might be expected (37 and 31°), because each pyridyl N atom is involved in an interaction with the nearby sulfur atom [N(1)···S(13) 2.778, N(26)···S(14) 2.724 Å]. It is well known that divalent sulfur (and also selenium) atoms can interact with both nucleophilic and electrophilic atoms giving short non-bonded contacts.[16–18] Nucleophilic atoms, such as the pyridyl nitrogen atoms in this structure, generally approach the sulfur atom of an S–X bond

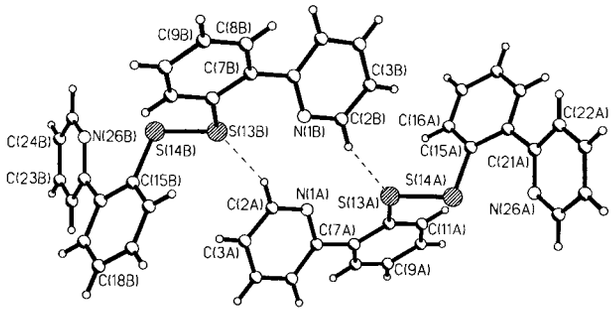

Fig. 1 Crystal structure of L–L, showing how two molecules associate across an inversion centre

Table 2 Selected bond lengths (Å) and angles (°) for L–L

N(1)–C(2)	1.334(2)	N(1)–C(6)	1.340(2)
C(6)–C(7)	1.476(2)	S(13)–S(14)	2.0603(6)
C(12)–S(13)	1.7918(14)	C(15)–S(14)	1.795(2)
C(20)–C(21)	1.483(2)	C(21)–N(26)	1.344(2)
C(25)–N(26)	1.339(2)		
C(2)–N(1)–C(6)	117.8(2)	C(11)–C(12)–S(13)	120.70(11)
C(12)–S(13)–S(14)	103.23(5)	S(13)–S(14)–C(15)	103.90(5)
S(14)–C(15)–C(16)	120.88(12)	C(21)–N(26)–C(25)	118.18(13)

Table 3 Selected bond lengths (Å) and angles (°) for complex **1a**

Ru–N(51)	2.048(6)	Ru–N(61)	2.061(6)
Ru–N(41)	2.078(6)	Ru–N(31)	2.086(7)
Ru–N(21)	2.110(7)	Ru–S(10)	2.352(2)
N(51)–Ru–N(61)	78.9(2)	N(51)–Ru–N(41)	92.6(2)
N(61)–Ru–N(41)	96.4(3)	N(51)–Ru–N(31)	92.1(2)
N(61)–Ru–N(31)	170.0(2)	N(41)–Ru–N(31)	79.4(3)
N(51)–Ru–N(21)	175.2(2)	N(61)–Ru–N(21)	99.2(2)
N(41)–Ru–N(21)	92.1(3)	N(31)–Ru–N(21)	90.0(3)
N(51)–Ru–S(10)	87.9(2)	N(61)–Ru–S(10)	88.7(2)
N(41)–Ru–S(10)	174.9(2)	N(31)–Ru–S(10)	95.5(2)
N(21)–Ru–S(10)	87.6(2)		

(where X denotes an atom to which sulfur is covalently bonded) in a direction corresponding to an elongation of that bond, which is because of the involvement of the S–X σ* orbital in the interaction; *i.e.* the Z···S–X moiety (where Z is the nucleophilic atom) is nearly linear.[16] In L–L such a linear approach of the pyridyl N atom to the S–S bond is not possible due to obvious steric constraints, but nevertheless the N···S–S angles are both just 11°. Recent theoretical studies have shown that these close contacts are due to an attractive electrostatic interaction between the S and Z atoms.[17] The N···S distances we observe are at the shorter end of the scale for such contacts (values of 2.9–3.0 Å are common) indicating that the interaction here is quite strong. One might expect that as a consequence of this N···S interaction the S–S bond would be lengthened due to the presence of electron density in its σ* orbital, but the S(13)–S(14) separation of 2.060 Å is not significantly different from the values found in other crystal structures of disulfides.[19] The second feature of interest is that two molecules of L–L are associated by C–H···S hydrogen bonding across an inversion centre (Fig. 1); the C···S separation is 3.672 Å, and the H···S separation is 2.79 Å.

The structure of complex **1a** is shown in Fig. 2; selected bond lengths and angles are in Table 3. The metal centre has the expected pseudo-octahedral geometry, with deviations from ideality arising from the constrained bite angles of the bidentate ligands. Whereas the bipy ligands are nearly-planar (inter-ring torsion angles are 5° for the bipy ligand containing rings 3 and 4, and 3° for that containing rings 5 and 6) the ligand L^- has a torsion angle of *ca.* 40° between the two aromatic rings. This is a conseqence of the formation of a six-

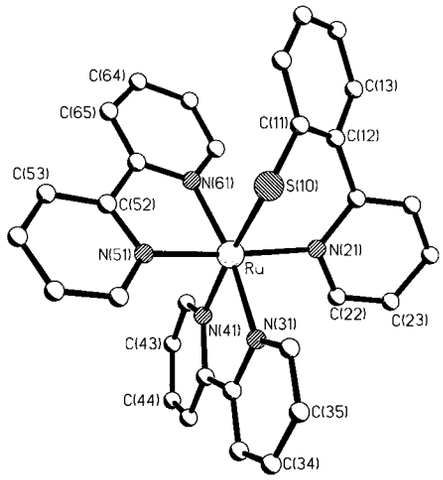

Fig. 2 Crystal structure of the cation of complex **1a**

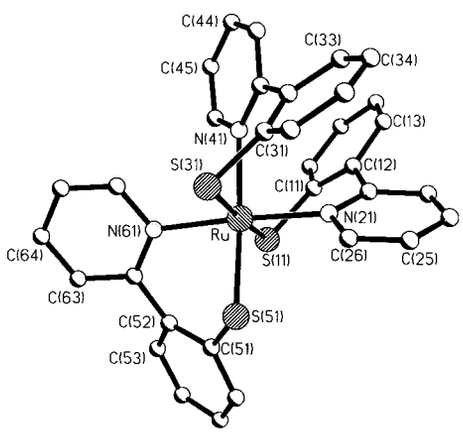

Fig. 3 Crystal structure of the complex of **2**·0.5CH_2Cl_2

membered chelate ring, and the fact that the lone pairs at the (formally) sp^3-hybridised S atom are directed out of the plane of the phenyl ring. Similar twists are common in complexes of related pyridine–phenol ligands.[6,7] The Ru–N distances span the range 2.048 − 2.110 Å {*cf.* 2.056 Å for $[Ru(bipy)_3]^{2+}$}.[20] Of these, Ru–N(21) is somewhat longer than the others. This is presumably a steric effect arising from the fact that the Ru–S and Ru–N bonds within the chelated ligand L^- have very different equilibrium distances; it is not possible for N(21) to co-ordinate as closely as it would like, given the greater length of the Ru–S bond. The Ru–S distance (2.352 Å) is typical of other ruthenium(II)–benzenethiolate bond lengths.[4] There is no significant *trans* effect involving the thiolate ligand: Ru–N(41) is not significantly different in length from the other four Ru–N bonds. Any lengthening of this bond that might be expected as a result of the negative charge *trans* to it is apparently offset by the increased Ru(d_π)→pyridyl(π^*) back bonding that can occur because of the greater electron density at the metal centre. Since these two competing effects tend to cancel out, ruthenium–pyridyl ligand distances are not so sensitive to changes in the electron density at the metal centre as are bonds to other ligands; for example the Ru–N (pyridyl) bond distances in $[Ru(bipy)_3]^{2+}$ and $[Ru(bipy)_3]^{3+}$ are virtually identical.[21]

The structure of complex **2** is shown in Fig. 3; selected bond lengths and angles are in Table 4. It has a meridional (rather than facial) configuration, which is more sterically favourable and generally occurs in complexes of asymmetric tris-chelate ligands. All three ligands are substantially twisted, for the reasons mentioned above, with torsion angles of about 40° in each case. The Ru–N bonds are significantly longer than those of other ruthenium(III)–pyridyl complexes, and are comparable to the Ru–N(41) bond of **1a** . This lengthening cannot result from a *trans* effect involving benzenethiolate ligands as all three Ru–N bonds are similarly affected, and the absence of such an effect was noted in the structure of **1a** above. It must therefore (as in **1a**) be a steric effect, in which the Ru–N bonds are stretched by the requirement of the Ru–S bonds to be relatively long (compared to the Ru–N distances). Further support for this is provided by two observations. First, the Ru–S distances involving S(11) and S(31) (the mutually *trans* pair) are not significantly different from the Ru–S(51) distance where S(51) is *trans* to a pyridyl ring, which suggests that the bond distances in this complex are more controlled by steric effects than electronic ones. Secondly, the Ru–S distances (2.32–2.35 Å) are not significantly different from that which was observed in **1a**, indicating that the expected contraction of the Ru–S bonds as the oxidation state of the metal increases is prevented by the steric crowding.

Table 4 Selected bond lengths (Å) and angles (°) for complex **2**·0.5CH_2Cl_2

Ru–N(21)	2.107(4)	Ru–N(61)	2.128(4)
Ru–N(41)	2.147(4)	Ru–S(11)	2.322(2)
Ru–S(31)	2.351(2)	Ru–S(51)	2.3486(13)
N(21)–Ru–N(61)	176.2(2)	N(21)–Ru–N(41)	90.4(2)
N(61)–Ru–N(41)	92.9(2)	N(21)–Ru–S(11)	87.96(12)
N(61)–Ru–S(11)	90.10(2)	N(41)–Ru–S(11)	90.31(11)
N(21)–Ru–S(51)	91.11(2)	N(61)–Ru–S(51)	85,75(11)
N(41)–Ru–S(51)	175.06(11)	S(11)–Ru–S(51)	94.44(5)
N(21)–Ru–S(31)	92.79(12)	N(61)–Ru–S(31)	89.39(12)
N(41)–Ru–S(31)	85.21(11)	S(11)–Ru–S(31)	175.46(5)
S(51)–Ru–S(31)	90.02(5)		

Table 5 Electrochemical and electronic spectral data for complexes **1** and **2**

Complex	$E_{\frac{1}{2}}^a$/V (ΔE_p/mV)	λ_{max}/nm ($10^{-3}\varepsilon$/dm^3 mol^{-1} cm^{-1})
1	+1.21,[b] −0.07 (70), −1.89 (100), −2.18 (120)[c]	578 (5.2), 497 (7.0), 366 (11), 296 (46), 222 (45)[c]
2	+0.56 (120), −0.21 (180), −1.34 (130)[d]	2320 (0.19), 1360 (0.08), 737 (6.4), 564 (1.5), 458 (3.7), 360 (sh, ≈7.1), 269 (43), 256 (53)[d]

[a] *vs.* Ferrocene–ferrocenium. [b] Irreversible. [c] Recorded in MeCN. [d] Recorded in CH_2Cl_2, apart from the near-IR transitions of the electronic spectrum which were recorded separately in $CDCl_3$.

Electrochemical studies

The electrochemical properties of complexes **1** and **2** are summarised in Table 5. They showed a variety of chemically reversible processes (*i.e.* cathodic and anodic peak currents had equal intensity over a wide range of scan rates); the greater-than-ideal peak–peak separations are ascribed to uncompensated solution resistance, particularly as the separations for **2** (which was studied in CH_2Cl_2) were significantly greater than those for **1** (which was studied in MeCN).

Metal-based couples. The metal-based couples are the features which are of most significance for assessing the electronic properties of the ligands. For the N_5S-co-ordinated **1** (N from pyridyl, S from benzenethiolate), the Ru^{II}–Ru^{III} couple occurs at −0.07 V *vs.* the ferrocene–ferrocenium couple, a substantial shift from the value of +0.89 V for $[Ru(bipy)_3]^{2+}$. Substitution of the pyridyl ligand by an anionic benzenethiolate has therefore stabilised the ruthenium(III) state by 0.96 V. In comparison, the Ru^{II}–Ru^{III} couple of $[Ru(bipy)_2(hpp)]^+$, with an N_5O donor set (O from phenolate), is shifted by 0.86 V with respect to $[Ru(bipy)_3]^{2+}$,[6] so the benzenethiolate stabilises the higher metal oxidation state by an additional 0.1 V compared to the phenolate ligand. There are two separate contributions to this 0.96 V stabilisation of the ruthenium(III) state. The first is the change in the overall charge on the complex; the +1 charge of **1** compared

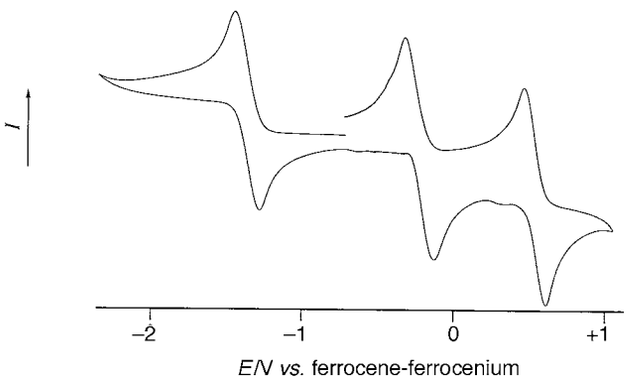

Fig. 4 Cyclic voltammogram of complex **2** in CH_2Cl_2, showing (from left to right) the Ru^{II}–Ru^{III} couple, the Ru^{III}–Ru^{IV} couple and the unexpected sulfur-based couple

to the +2 charge of $[Ru(bipy)_3]^{2+}$ means that removal of an electron will be electrostatically much easier in the former case, irrespective of the nature of the ligand donor set. The second contribution arises from the inherently different electron donor/acceptor properties of a benzenethiolate ligand compared to a pyridyl ligand. Although it is not possible to separate the two effects, it has been suggested that the electrostatic effect is the more significant, with changes in the nature of the ligands taking second place.[5]

Since $[Ru(bipy)_2(hpp)]^+$, like **1**, carries a +1 charge it follows that the electrostatic contribution to stabilisation of the ruthenium(III) state will be similar in both cases. The additional +0.1 V stabilisation of the ruthenium(III) state in **1** compared to $[Ru(bipy)_2(hpp)]^+$, therefore, may be ascribed to the different electronic properties of the sulfur and oxygen ligands, and apparently suggests that the benzenethiolate is a slightly stronger electron donor than is phenolate. This is inconsistent with the known σ-donor abilites of these ligands based on their affinities for protons: the pK_a values for protonation of phenolate and benzenethiolate are 10 and 6.5 respectively, indicating that phenolate should be the stronger electron donor. However such a simplistic electrostatic picture ignores the effects of covalency, in particular the greater polarisability of the lone-pair electrons on sulfur compared to those on oxygen, which is clearly a dominant effect here.

For complex **2** (N_3S_3 donor set) there are, surprisingly, *three* one-electron redox processes at moderate potentials (Fig. 4, Table 5); in contrast $[Ru(hpp)_3]$ (N_3O_3 donor set) shows two waves corresponding to Ru^{II}–Ru^{III} and Ru^{III}–Ru^{IV} couples. The Ru^{II}–Ru^{III} couple of **2** may be ascribed to the process at −1.43 V; for $[Ru(hpp)_3]$ this couple occurred at −1.39 V. The difference between the electronic effects of phenolate and benzenethiolate donors is less obvious here, with the two complexes having their Ru^{II}–Ru^{III} couples at very similar potentials. The negative shift of 2.32 V with respect to $[Ru(bipy)_3]^{2+}$ corresponds to 0.77 V per benzenethiolate donor, which is somewhat smaller than the shift of 0.96 V observed for **1**. When significant covalency is involved we would not necessarily expect the effects to be exactly additive. For example, in complex **2**, where there are three polarisable benzenethiolate donors, it is quite reasonable that each one should donate rather less electron density to the metal than does the single such donor of **1** (the electroneutrality principle), and this is reflected in the electrochemical results.

Steifel and co-workers[5] reported a few years ago the syntheses and electrochemical properties of a series of complexes in which two sulfur-based ligands were attached to a $\{Ru(bipy)_2\}^{2+}$ fragment, and these provide a convenient basis for comparison with **1** and **2**. The potential of the Ru^{II}–Ru^{III} couple of $[Ru(bipy)_2(SPh)_2]$ was −0.15 V *vs.* SCE, *i.e.* −0.52 V *vs.* ferrocene–ferrocenium, a shift of 1.41 V from $[Ru(bipy)_3]^{2+}$ or about 0.7 V per benzenethiolate substituent, which is in good agreement with the behaviour of **2** and less good but still reasonable agreement with **1**.

The couple at −0.21 V *vs.* ferrocene–ferrocenium for complex **2** we assign to the expected Ru^{III}–Ru^{IV} couple, by comparison with $[Ru(hpp)_3]$ for which this couple occurs at +0.14 V.[6] The ruthenium(IV) state is therefore stabilised in **2** by 0.35 V more than it is in **1**. This difference in potential between the Ru^{III}–Ru^{IV} couples is much larger than the difference between the Ru^{II}–Ru^{III} couples for the same pair of complexes (0.04 V in the same sense). The better electron-donating properties to ruthenium of benzenethiolate over phenolate therefore become more pronounced as the oxidation state of the metal centre increases, which is consistent with the fact that the electrons on sulfur are more polarisable than those on oxygen: the benzenethiolate ligands can adjust to the higher oxidation state by transferring more electron density to the metal, which the more electronegative and less polarisable oxygen atoms are unable to do so well.

Ligand-based couples. The third redox process of complex **2**, at +0.56 V, was entirely unexpected as it has no counterpart in $[Ru(hpp)_3]$. It is highly unlikely to be a Ru^{IV}–Ru^{V} couple as ruthenium(V) complexes of any sort are very rare and are unknown with ligands of this type. It must therefore be ligand based, which raises the question of why it was not apparent in **1** (which has just an irreversible oxidation at +1.21 V, assigned to oxidation of the single sulfur atom),[22] and in the voltammogram of the free L–L (see below). A possible answer is provided by the observation that 'odd-electron sigma-bonds', of formal order 0.5, can be formed by one-electron oxidation of two initially non-bonded atoms which both have lone pairs: *i.e.* on oxidation of one member of a pair of intially non-interacting molecules such as R_2S an adduct $[R_2S\cdots SR_2]^{\cdot+}$ can form[22–25] with (computed) S···S separations of around 2.8 Å.[24] There is a simple molecular orbital rationale for this. If two atomic orbitals, each containing a lone pair, overlap slightly then bonding and antibonding sum-and-difference combinations will form. Normally both of these contain two electrons so there is no net bonding interaction, but one-electron oxidation of the pair will give a $(\sigma)^2(\sigma^*)^1$ configuration, *i.e.* a three-electron hemi-bond. This interaction has been shown to be particularly strong for a pair of sulfur atoms, with a computed bond-dissociation energy of 111 kJ mol^{-1} for $[H_2S\cdots SH_2]^{\cdot+}$,[24] and several such species have been prepared chemically and spectroscopically characterised in solution.[25] In **1** therefore the lone sulfur atom oxidises to a radical cation and, since the oxidation is irreversible, then reacts further in some way. In **2**, however, sulfur-centred oxidation is facilitated (*i.e.* the oxidation potential is much lower) and the product stabilised (*i.e.* the oxidation is chemically reversible on the electrochemical time-scale) by interaction of the sulfur radical cation with an adjacent sulfur atom in the co-ordination sphere of the complex to give a hemi-bonded pair. Presumably S(51) is the most likely site of oxidation as it has two neighbouring sulfur atoms in positions *cis* to it. The S(11)···S(51) and S(31)···S(51) distances (3.43 and 3.32 Å respectively) are considerably larger than the value of *ca.* 2.8 Å for an optimum interaction, but a weak interaction could occur over this distance and anyway it is quite possible that the co-ordination sphere of the complex could distort to allow the interacting sulfur atoms to approach each other more closely. Complex **1** also shows two reversible ligand-centred processes which we assign to the bipyridyl ligands (Table 5); these are absent for **2**.

We also examined the electrochemical properties of the disulfide L–L in CH_2Cl_2. No reductions were observed out to the limit of the solvent window (−2.4 V *vs.* ferrocene–ferrocenium), which was surprising in view of the fact that L–L undergoes reductive cleavage on co-ordination to ruthenium. It was therefore not possible to generate electrochemically the free anion L^- to assess its electrochemical behaviour and compare it with that

of co-ordinated L. To positive potentials a broad, totally irreversible oxidation wave was observed at *ca.* +1.2 V, near the limit of the accessible potential window, which is consistent with a sulfur-based process.

Electronic spectral properties

The electronic spectrum of complex **1** (Table 5) is similar to that of the N_5O analogue $[Ru(bipy)_2(hpp)]^+$, and may be assigned in the same way.[6] The reduced ligand-field strength and lower symmetry of **1** compared to that of $[Ru(bipy)_3]^{2+}$ has two effects: the d_π orbitals are raised in energy, and rendered substantially inequivalent. The result of this is that the expected metal-to-ligand charge-transfer (m.l.c.t.) transitions from the filled metal d_π manifold to the empty ligand-based π* levels are moved to lower energy, and also spread out to cover a wide range of energies. Thus m.l.c.t. transitions for **1** occur at 578 and 497 nm, compared to *ca.* 450 nm for $[Ru(bipy)_3]^{2+}$. The high-energy ligand-centred $\pi \longrightarrow \pi^*$ transitions are also apparent at 296 and 222 nm. The transition at 366 nm is probably a higher-energy m.l.c.t. process.

The spectrum of complex **2** in the visible region (Table 5) is dominated by a sharp, strong band at 737 nm which, considering the presence of polarisable sulfur ligands and an oxidised metal centre with a hole in the d_π manifold, is likely to be a sulfur-to-Ru^{III} ligand-to-metal charge-transfer (l.m.c.t.) process. Pyridyl-to-Ru^{III} l.m.c.t. transitions would also be expected at around this position but are generally much less intense than this transition and are likely to be obscured by it.[26] The direction of this charge transfer (from sulfur to ruthenium) indicates that the highest-energy sulfur orbitals lie below the metal d_π orbitals, which is consistent with the order of redox processes that we proposed earlier (*i.e.* the Ru^{III}–Ru^{IV} couple for **2** occurs before the ligand-based process). There are also three poorly resolved transitions at 564, 458 and 360 nm the nature of which is uncertain, as well as a ligand-centred π–π* transition at 269 nm.

Owing to the d_π^5 configuration of Ru^{III}, and the inequivalence of the three d_π orbitals due to the low symmetry of the complex, two very low energy d–d transitions are expected arising from transitions within this orbital set.[27] For $[Ru^{III}(hpp)_3]$, with a *mer*-N_3O_3 donor set, these occurred at 1500 and 2100 nm with absorption coefficients of around 100 $dm^3\ mol^{-1}\ cm^{-1}$.[7] The spectrum of **2** in the near-IR region (using $CDCl_3$ as solvent to avoid C–H overtone bands) showed these two transitions at 1360 and 2320 nm.

Conclusion

The bidentate N,S-donor ligand HL has been isolated as the disulfide dimer L–L, which was used directly to prepare $[Ru^{II}(bipy)L][PF_6]$ **1** and $[Ru^{III}L_3]$ **2**. The electrochemical properties of these complexes, and the electronic spectrum of **2**, show that the polarisable benzenethiolate ligands are more effective electron donors to ruthenium (+2 and +3) than are phenolates.

Acknowledgements

We thank the EPSRC for financial support.

References

1 A. M. W. Cargill Thompson, J. C. Jeffery, D. J. Liard and M. D. Ward, *J. Chem. Soc., Dalton Trans.*, 1996, 879; D. A. Bardwell, J. C. Jeffery and M. D. Ward, *J. Chem. Soc., Dalton Trans.*, 1995, 3071; D. A. Bardwell, A. M. W. Cargill Thompson, J. C. Jeffery, E. E. M. Tilley and M. D. Ward, *J. Chem. Soc., Dalton Trans.*, 1995, 835; D. A. Bardwell, J. C. Jeffery, E. Schatz, E. E. M. Tilley and M. D. Ward, *J. Chem. Soc., Dalton Trans.*, 1995, 825; J. C. Jeffery, J. P. Maher, C. A. Otter, P. Thornton and M. D. Ward, *J. Chem. Soc., Dalton Trans.*, 1995, 819.
2 W. Kaim and B. Schwederski, *Bioinorganic Chemistry: Inorganic Elements in the Chemistry of Life*, Wiley, Chichester, 1994, and refs. therein.
3 D. Sellmann, G. Mahr and F. Knoch, *Inorg. Chim. Acta*, 1994, **224**, 35; S. Brooker and P. D. Croucher, *J. Chem. Soc., Chem. Commun.*, 1995, 1493; U. Brand and H. Vahrenkamp, *Chem. Ber.*, 1995, **128**, 787; J. E. Barclay, D. J. Evans, G. Garcia, M. D. Santana, M. C. Torralba and J. M. Yago, *J. Chem. Soc., Dalton Trans.*, 1995, 1965; R. Hahn, A. Nakamura, K. Tanaka and Y. Nakayama, *Inorg. Chem.*, 1995, **34**, 6562.
4 S. P. Satsangee, J. H. Hain, jun., P. T. Cooper and S. A. Koch, *Inorg. Chem.*, 1992, **31**, 5160; D. Sellmann, O. Käppler and F. Knoch, *J. Organomet. Chem.*, 1989, **367**, 161; D. Sellmann, P. Lechner, F. Knoch and M. Moll, *J. Am. Chem. Soc.*, 1992, **114**, 922; L. D. Field, T. W. Hambley and B. C. K. Yau, *Inorg. Chem.*, 1994, **33**, 2009; P. G. Jessop, S. J. Rettig, C.-L. Lee and B. R. James, *Inorg. Chem.*, 1991, **30**, 4617; S.-L. Soong, J. H. Hain, jun., M. Millar and S. A. Koch, *Organometallics*, 1988, **7**, 556.
5 M. A. Greaney, C. L. Coyle, M. A. Harmer, A. Jordan and E. I. Steifel, *Inorg. Chem.*, 1989, **28**, 912.
6 B. M. Holligan, J. C. Jeffery, M. K. Norgett, E. Schatz and M. D. Ward, *J. Chem. Soc., Dalton Trans.*, 1992, 3345.
7 D. A. Bardwell, D. Black, J. C. Jeffery, E. Schatz and M. D. Ward, *J. Chem. Soc., Dalton Trans.*, 1993, 2321.
8 C. M. Duff and G. A. Heath, *Inorg. Chem.*, 1991, **30**, 2528.
9 A. Juris, V. Balzani, F. Barigeletti, S. Campagna, P. Belser and A. von Zelewsky, *Coord. Chem. Rev.*, 1988, **84**, 85.
10 J. W. Haworth, I. M. Heilbron and D. H. Hey, *J. Chem. Soc.*, 1940, 339.
11 B. P. Sullivan, D. J. Salmon and T. J. Meyer, *Inorg. Chem.*, 1978, **17**, 3334.
12 D. McKinnon, K. A. Duncan, A. M. McKinnon and P. A. Spevack, *Can. J. Chem.*, 1985, **63**, 882.
13 SHELXTL 5.03 program system, Siemens Analytical X-Ray Instruments, Madison, WI, 1995.
14 A. M. W. Cargill Thompson, S. R. Batten, J. C. Jeffery, L. H. Rees and M. D. Ward, *Aust. J. Chem.*, in the press.
15 K. S. Finney and G. W. Everett, *Inorg. Chim. Acta*, 1974, **11**, 185.
16 R. E. Rosenfeld, jun., R. Parthasarathy and J. D. Dunitz, *J. Am. Chem. Soc.*, 1977, **99**, 4860.
17 F. T. Burling and B. M. Goldstein, *J. Am. Chem. Soc.*, 1992, **114**, 2313.
18 F. T. Burling and B. M. Goldstein, *Acta Crystallogr., Sect. B*, 1993, **49**, 738; G. R. Desiraju and V. Nalini, *J. Mater. Chem.*, 1991, **1**, 201; D. Britton and J. D. Dunitz, *Helv. Chim. Acta*, 1980, **63**, 1068; M. Iwaoka and S. Tomoda, *J. Am. Chem. Soc.*, 1996, **118**, 8077.
19 F. H. Allen, O. Kennard, D. G. Watson, L. Brammer, A. G. Orpen and R. Taylor, *J. Chem. Soc., Perkin Trans. 2*, 1987, S1.
20 D. P. Rillema, D. S. Jones and H. A. Levy, *J. Chem. Soc., Chem. Commun.*, 1979, 849.
21 D. W. Phelps, E. M. Kahn and D. J. Hodgson, *Inorg. Chem.*, 1975, **14**, 2486.
22 K.-D. Asmus, *Acc. Chem. Res.*, 1979, **12**, 436.
23 T. Clark, *J. Am. Chem. Soc.*, 1988, **110**, 1672.
24 P. M. W. Gill and L. Radom, *J. Am. Chem. Soc.*, 1988, **110**, 4931.
25 M. Bonifacic and K.-D. Asmus, *J. Org. Chem.*, 1986, **51**, 1216; M. Bonifacic, J. Weiss, S. A. Chaudri and K.-D. Asmus, *J. Phys. Chem.*, 1985, **89**, 3910; M. Göbl, M. Bonifacic and K.-D. Asmus, *J. Am. Chem. Soc.*, 1984, **106**, 5984.
26 G. M. Bryant and J. E. Ferguson, *Aust. J. Chem.*, 1971, **24**, 275; R. J. P. Williams, *J. Am. Chem. Soc.*, 1953, **75**, 2163.
27 G. K. Lahiri, S. Bhattacharya, B. K. Ghosh and A. Chakravorty, *Inorg. Chem.*, 1987, **26**, 4324.

Received 27*th September* 1996; *Paper* 6/06650J